MINERAL DISTRIBUTION IN RESERVOIR ROCKS AND ITS IMPACT ON ENHANCED OIL RECOVERY

James J. Howard and Gary L. Lovell
ConocoPhillips

This paper was prepared for presentation at the International Symposium of the Society of Core Analysts held in Austin, Texas, USA 18-21 September, 2011

ABSTRACT

Estimates of bulk mineralogy and the relationships in their distribution relative to other grains and pores were done with SEM-based data acquisition and image analysis software. Minerals are identified by their EDS spectra, with varying degrees of tolerance allowed in the assignment to account for compositional variability and acquisition conditions. The bulk mineralogy results are robust when compared with conventional XRD-generated values. Image processing and analysis generated mineral- specific grain-size distributions and nearest neighbor information. The key result is the identification of the mineralogy that is adjacent to pore space. Clay minerals are easily distinguished from other aluminosilicates and are often the predominant mineralogy lining the pore walls. A series of low-salinity waterflood tests on sandstones with uniform total clay mineral contents showed increased oil production in samples with higher clay mineral concentrations adjacent to the pores.

INTRODUCTION

The question of how minerals are distributed in porous media, especially those adjacent to the pores, has interested researchers for many years. Descriptions of mineral diagenesis and formation damage abound in the literature and have helped to develop an understanding of the importance of a more detailed and quantitative characterization of the distribution of minerals. This information is particularly critical since fluid-rock interactions, whether they are diagenetic reactions that alter the pore geometry or processes that affect multiphase fluid flow, (e.g. wettability) are obviously restricted to the fluid-rock interface. The role of pore wall chemistry is critical in multiphase flow in porous media, and their petrophysical characterization, perhaps none so more than their NMR response [1].

Traditional assessment of mineralogy normally yields a result of bulk properties. Yet any cursory investigation of a rock under a microscope reveals a non-uniform distribution of minerals, a result of original depositional processes and post-depositional diagenetic reactions. The development of quantitative spatial information lagged until suitable image processing algorithms were created [2]. Image processing of petrographic thin sections was suitable for the relationships amongst grains, but automated mineral identification was much more challenging. The development of mineral identification procedures based on scanning electron microscope (SEM) images provided a more

certain method for discriminating amongst different minerals by taking advantage of the compositional information available in these images. Back-scattered X-rays (BSE) or Energy Dispersive X-ray spectra (EDS) respond to compositional differences in the minerals. A number of approaches have been proposed for applying EDS elemental information to mineral identification and quantification [3-5]. This study was based on matching complete elemental spectra to a set of end-member compositions [6].

METHODS

Standard samples were prepared for 2-D SEM imaging by filling the pore space with low-viscosity epoxy, polishing the sample surface and coating with carbon. Images were collected with a JEOL 8200 microprobe under software control for data acquisition (MLA, FEI Company). MLA has a number of approaches to collect data for mineralogical analysis. The method chosen for this study used a combination of BSE that distinguished minerals from void (epoxy-filled) and then directed the instrument to collect EDS spectra at multiple points on the minerals. Since segmentation of minerals based on BSE images only was quite difficult because of compositional similarities, the strategy was to collect an EDS spectrum at each non-void point on a high-resolution grid. Several EDS spectra were collected for each major phase in order to provide some robustness in identifying the unknown spectra. Each EDS point was assigned to an end-member phase by comparison of the full spectra against the standards, with final grouping taking place during the data analysis stage. Once a set of standards and grouping classes was established for one sample, the process was repeated for the remaining samples in the suite.

RESULTS

Mineral maps were generated for several sandstone suites used in EOR-related laboratory tests. Modal mineralogy from the SEM-based measurements was compared with values generated by X-Ray powder diffraction (XRD) analysis that used Rietveld modeling techniques. The XRD values were treated as the baseline for any comparisons, though they too were subject to uncertainty and imprecise phase identification. One area where the SEM-based analysis had an advantage was the identification and quantification of trace minerals, where an individual grain was counted by the SEM even when it fell below the standard XRD detection level of 0.5 wt%.

Sandstone set A was characterized by a complex mineralogy and pore system that offered many challenges in mineral identification. The SEM-based mineralogy overstated the presence of the clay minerals, illite and glauconite, while underestimating quartz. Siderite and the small amounts of feldspar in these samples generally matched the values generated by XRD. This was the first set studied and it was determined later that the grid size for individual EDS analysis of the BSE image was much too coarse for these samples. Compositional similarities amongst the various clay minerals and feldspars made classification of individual points difficult. In this early example too many standards were defined, which resulted in the need to group more phases into the final end-member mineralogy. Subsequent studies used fewer standards and allowed the

pattern recognition algorithms in the classification software more flexibility in assigning final mineralogy. The images were also collected at a lower magnification than subsequent runs, which resulted in considerable overlap of grains within a single voxel that complicated the collected spectra.

Sandstone set B was composed of feldspar-rich sand with several clay minerals and zeolites present. SEM-based and XRD estimates of quartz were very close (Figure 1a). The SEM-based estimates of different feldspars, K-feldspar and Na-plagioclase, showed trends with the XRD values, though not a 1:1 relationship. The combination into a total feldspar abundance, however, did compare favorably (Figure 1b). The clay minerals included illite and chlorite, with several samples containing up to 10 wt % of the zeolite, laumontite. The SEM-based total clay mineral abundance was for the most part comparable with estimates from XRD (Figure 1c).

Sandstone set C was compositionally simpler, with quartz, feldspars and illite as the dominant minerals. The comparison with XRD values was similar to those in set B (Figure 1). While the total clay mineral content for these samples was relatively low compared to other samples, the distribution of these clay minerals was distinctive. The mineral maps illustrated the most of the illite was located on the surfaces of the grain-pore interface (Figure 2). The images also suggested that the illite was predominantly distributed on the surfaces of larger pores. The image was generated with a high-resolution grid of 2 micron step sizes between EDS points and at higher magnification than the sample A suite. A test of grid resolution showed that larger step sizes generated comparable bulk mineralogy estimates, but with a loss of mineral map resolution. The accompanying back-scattered image showed the limited contrast in phase composition and highlighted the challenges in the segmentation of individual grains by BSE only.

The general agreement between XRD and SEM mineral estimates was due in part to high quality XRD results, large number of SEM sample points (>10,000) and accurate phase identification with the EDS spectra. Even so, mineral families required grouping in order to reach this level of agreement.

While descriptions of clay mineral distribution on the surfaces of grains are common, the proportion of clay mineral available for reaction, or conversely the proportion of pore wall surfaces coated with sensitive clay minerals has not been quantified on a regular basis. The nearest-neighbor relationship between the identified phases, including the porosity, was extracted from the mineral maps.

Set A was used in a low-salinity waterflood experiment where the amount of incremental oil produced upon the introduction of a tertiary low-salinity flood was recorded. These samples showed considerable variability in the effectiveness of the low-salinity process. Previous work suggested that total clay mineralogy could be a predictor of low-salinity effectiveness [7], but for these samples there was no obvious correlation (Figure 3a). When the proportion of pore surface in contact with total clay minerals was compared

against the incremental change in water saturation due to low-salinity related production a more positive correlation was revealed (Figure 3b). The composition of the pore walls, (i.e. minerals adjacent to the pore space) was dominated by quartz, glauconite, and siderite with small amounts of other phases (Table 1).

Set B also showed a positive correlation between the change in original oil in place due to tertiary low-salinity waterflood and the portion of the pore surface associated with clay minerals. Set C also showed significant oil production following low-salinity water imbibition despite the low values of total clay mineral content. As apparent in the mineral maps, the relatively small amount of illite dominated the pore wall surfaces.

CONCLUSION

SEM-based mineral maps have the potential to replicate the mineralogy values obtained from conventional XRD methods on bulk samples, while also providing insights into the distribution of minerals, particularly those adjacent to the pores. The SEM-based methods still require development to improve their reproducibility, but the several micron resolution provides the opportunity for high-resolution images. High magnification images coupled with high-resolution EDS grids resulted in significantly higher quality mineral maps, justifying the increased time required for data acquisition. The composition of the grain-pore interface undoubtedly is an important factor in understanding mechanisms of enhanced oil recovery processes.

REFERENCES

1. Basan, P., Howard, J., Lahann, Pritchard, T., Attard, J. and Camden, D. “Variations in NMR relaxativity and its relationship with pore size in sandstones from the South Morecambe field, Irish Sea” *Proceedings of 16th European Formation Evaluation Symposium* (1994) Society of Professional Well Log Analysts, paper AA.

2. Russ, J. *The Image Processing Handbook*, 5th Ed., Taylor & Francis, Boca Raton, Fl. (2007) 817pp.

3. Togami, S., Takano, M., and Kumazawa, M. “An algorithm for the transformation of XRF images into mineral distribution maps”. *The Canadian Mineralogist* (2000) **38** 1283-1294.

4. Tsuji, T., Yamaguchi, H, Ishii, T., and Matsuoka, T. “Mineral classification from quantitative X-ray maps using neural network: Application to volcanic rocks”. *Island Arc* (2010) **19**, 105-119.

5. Prêt, D., Sammartino, S., Beaufort, D., Meunier, A., Fialin, M., and Michot, L. ”A new method for quantitative petrography based on image processing of chemical element maps: part I.. Mineral mapping applied to compacted bentonites”. *Amer. Min*. (2010) **95**, 1379-1388.

6. Fandrich, R., Gu, Y,, Burrows, D., and Moeller, K. “Modern SEM-based mineral liberation analysis”. *Int. J. Miner. Process* (2007) **84**, 310-320.

7. Lager, A., Webb, K., Black, C., Singleton, M., and Sorbie, K. “Low salinity oil recovery – an experimental investigation” *Petrophysics* (2008) **49**, 28-35.

Table 1. Mineral composition adjacent to porosity.

Sample	Quartz	Glauconite	Siderite
A-1	9.9	55.4	34.6
A-2	12.8	52.1	35.0
A-3	20.9	27.9	50.9
A-4	53.6	45.1	0.1
A-5	14.6	42.6	42.6
A-6	9.4	57.3	33.2
A-7	39.1	30.2	30.7
A-8	59.8	39.7	0.2
A-9	17.8	38.2	43.8
A-10	45.5	53.3	0.6
A-11	9.9	55.4	34.6
A-12	21.3	41.0	37.4
A-13	35.6	42.7	21.6
A-14	12.8	52.1	35.0
A-15	39.9	36.3	23.6
A-16	13.3	43.8	42.8
A-17	32.6	48.2	18.8
A-18	35.6	42.7	21.6

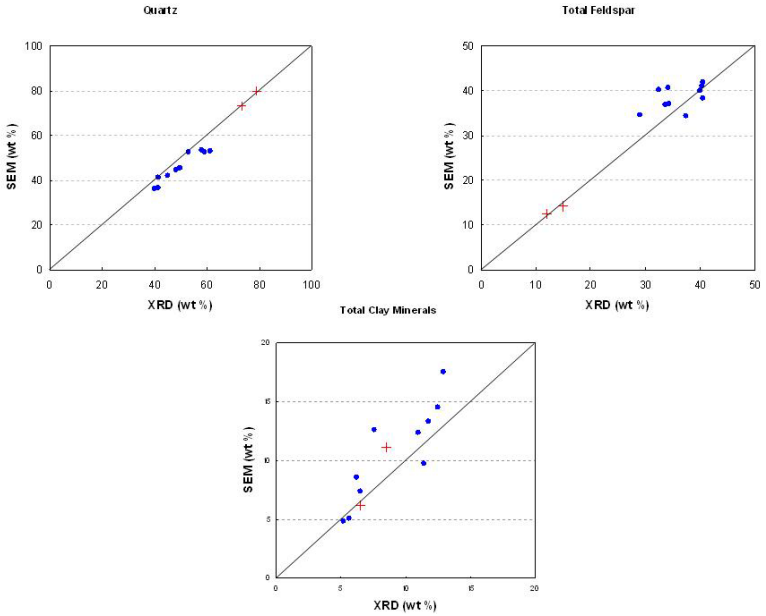

Figure 1 (a-c). Comparison of mineralogy estimates from standard XRD and SEM-based methods for (a) quartz, (b) total feldspars and (c) total clay minerals. The comparison includes samples from sandstone sets B (filled circles) and C (pluses)

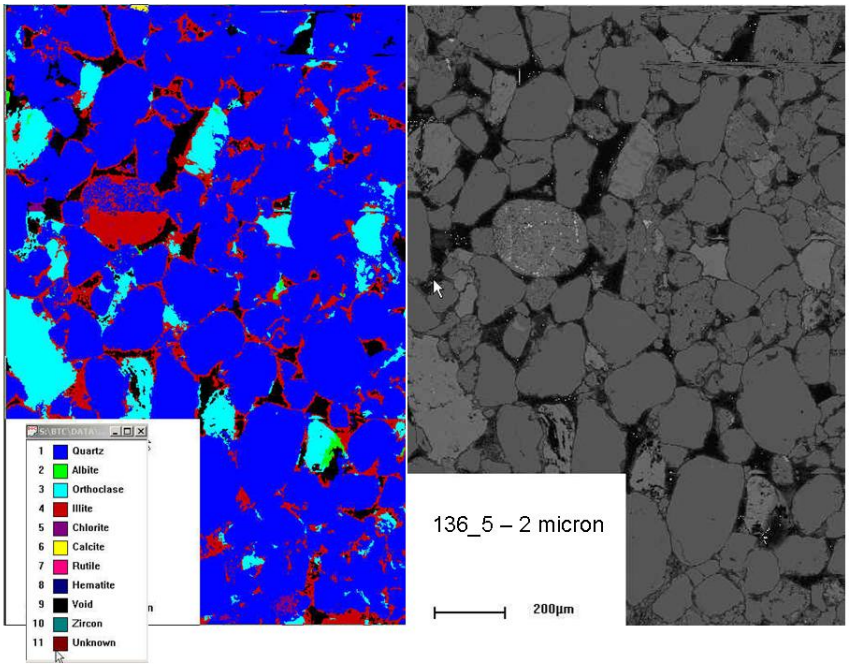

Figure 2. Mineral map of illite-coated pore walls for sandstone C sample(left) and the initial BSE image (right) used to segment grains (shades of gray) from pores (black).

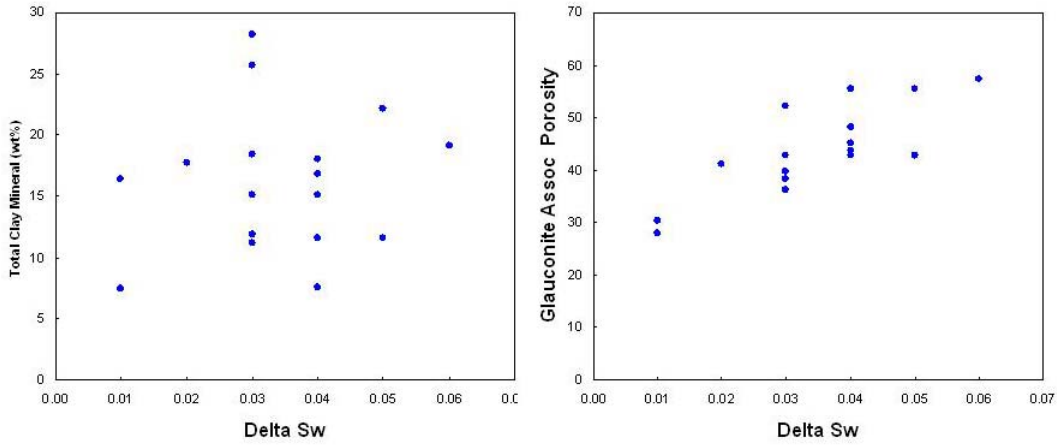

Figure 3. Change in water saturation due to incremental oil recovery following tertiary low-salinity waterflood in sandstone A samples does not correlate with total clay mineral content (a), but does show a good trend with the amount of glauconite adjacent to the pores.